A structural model for metallic glasses

DANIEL B. MIRACLE

Materials and Manufacturing Directorate, Air Force Research Laboratory, Wright-Patterson Air Force Base, Ohio 45433, USA
e-mail: Daniel.miracle@wpafb.af.mil

Despite the intense interest in metallic glasses for a variety of engineering applications, many details of their structure remain a mystery. Here, we present the first compelling atomic structural model for metallic glasses. This structural model is based on a new sphere-packing scheme—the dense packing of atomic clusters. Random positioning of solvent atoms and medium-range atomic order of solute atoms are combined to reproduce diffraction data successfully over radial distances up to ~1 nm. Although metallic glasses can have any number of chemically distinct solute species, this model shows that they contain no more than three topologically distinct solutes and that these solutes have specific and predictable sizes relative to the solvent atoms. Finally, this model includes defects that provide richness to the structural description of metallic glasses. The model accurately predicts the number of solute atoms in the first coordination shell of a typical solvent atom, and provides a remarkable ability to predict metallic-glass compositions accurately for a wide range of simple and complex alloys.

Although the first amorphous metal was discovered over 40 years ago[1], there is still no atomic structural model for the commercially and technologically important family of metallic glasses. Early structural models were based on randomness[2–4], but were modified to acknowledge that the nearest-neighbour atomic environment displayed order similar to that in competing crystalline structures[5–8]. However, attempts to define the structure of metallic glasses beyond the nearest-neighbour shell have continued to be unsuccessful. Building outwards from a unit cluster through attachment of additional clusters[5,6] introduces objectionable free volume due to packing frustration, and does not provide a basis for observed medium-range order (MRO). Although simple chemical twinning[7] can overcome these problems, agreement with measured MRO requires an arbitrary adjustment of domain size and includes an exceptionally large value for the metalloid–metalloid separation. These early efforts were directed at a description of metal–metalloid glasses, and extension to glasses with more than a single solute species or with solutes of different sizes and concentrations introduces significant conceptual and analytical difficulties. Recent work generalizes the description of local structure[9–11], but provides no new insights beyond the nearest-neighbour shell.

The present work describes a structural model for metallic glasses that extends well beyond the nearest-neighbour shell. Efficiently packed solute-centred atomic clusters[9,12,13] are retained as local structural elements. An extended structure is produced by idealizing these clusters as spheres and efficiently packing these sphere-like clusters to fill space. Face-centred cubic (f.c.c.) or hexagonal close-packed (h.c.p.) cluster packings are favoured, because they fill space most efficiently[14]. Further, f.c.c./h.c.p. packing of solute-centred atomic clusters introduces a physical basis for the experimentally observed solute ordering beyond the nearest-neighbour shell[15–18]. It is not likely that order of the cluster-forming solutes will extend beyond a few cluster diameters as a result of internal strains, as discussed below. Thus, just as a small deviation from the preferred inter-tetrahedral Si–O–Si bond angle is sufficient to destroy long-range order in silicate glasses[8,19], internal strains degrade long-range order in cluster packing in the present model. Adjacent clusters share solvent atoms in common faces, edges or vertices so that neighbouring clusters overlap in the first coordination shell. Although face sharing is preferred to minimize volume, internal strains introduce some amount of edge and vertex sharing. There is no orientational order amongst the clusters, so that the solvent atoms occupy random positions in this structure. This provides an
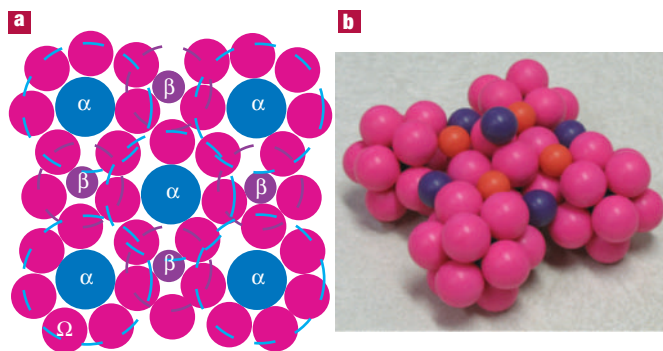
Figure 1 Illustrations of portions of a single cluster unit cell for the dense cluster packing model. **a**, A two-dimensional representation of a dense cluster-packing structure in a (100) plane of clusters illustrating the features of interpenetrating clusters and efficient atomic packing around each solute. Relaxations outside the plane of view cannot be shown in this two-dimensional representation. **b**, A portion of a cluster unit cell of a <12-10-9> model system representing a Zr-(Al,Ti)-(Cu,Ni)-Be alloy. The α sites are occupied by blue spheres, the β sites are occupied by purple spheres and the γ sites are occupied by orange spheres. Pink Zr solvent spheres form relaxed icosahedra around each α solute. There is no orientational order amongst the icosahedral clusters.

important distinction from the icosahedral glass model proposed for quasicrystalline structures[20].

In addition to solvent atoms Ω and the primary cluster-forming solute species α, cluster ordering introduces two additional topologically distinct solutes—a secondary (β) solute that occupies cluster-octahedral interstices and a tertiary (γ) solute that occupies cluster-tetrahedral interstices. This structural model therefore contains only four topologically distinct atomic constituents. The preferred size of α atoms relative to Ω is given by the discrete solute-to-solvent radius ratios R^* that produce efficient local packing in solute-centred atomic clusters[9]. Although it is tempting to calculate directly the size of the β and γ interstices between primary clusters, different cluster radii are obtained for vertex-, edge- and face-sharing of adjacent primary clusters, producing different sizes for β and γ interstices. Further, explicit account of the discrete non-spherical nature of the cluster surface and atomic relaxations must be made. Thus, these considerations do not provide useful insight into the specification of β and γ solute sizes. However, it has been shown that solute sizes that enable efficient atomic packing in the first coordination shell are strongly preferred for all solutes in metallic glasses[9], and so it is a fundamental feature of this model that β and γ solutes also possess discrete sizes R^* relative to solvent atoms. The dense cluster-packing structure thus comprises interpenetrating arrays of efficiently packed solute-centred clusters (Fig. 1).

Even though long-range solute ordering is not included in the present model, it is nevertheless useful to consider a unit cell of regularly positioned clusters as a representative structural element that extends over a restricted length scale. This enables the use of crystallographic terminology to describe atomic structure and packing over a medium-range length scale. Thus, distances can be calculated along <100>, <110> and <111> unit directions of an idealized f.c.c. cluster unit cell, and a cluster unit cell length Λ_0 can be calculated (see Methods). Because different solutes and clusters exist along these directions, different values of Λ_0 are generally obtained, so that the structure is internally strained. Λ_0 is controlled by the direction that produces the largest value in the most densely packed (that is, face-sharing) configuration. <111> is most often the controlling direction, so that

tensile strains exist along <100> and <110>. As α, β and γ clusters occur along <111>, face-sharing is typically obtained for adjacent unlike clusters along this direction. The <110> direction comprises adjacent α clusters whereas α and β clusters alternate along <100>, and vertex or edge sharing is favoured along these directions to reduce the tensile strains. Values of Λ_0 depend on the relative atomic sizes R (solute radius/solvent radius) and site occupancy, and typically fall in the range of 0.6 nm to 1.1 nm for the systems considered here.

Structural chemistry provides specific information regarding the relative number of sites (stoichiometry or concentration) and the relative sizes of constituent atoms in inorganic crystalline structures. In a similar way, the present model gives specific information on the relative sizes and relative number of sites, enabling comparison with the topologies (sizes and concentrations of constituent atoms) of known metallic glasses. Consider a system where α solutes have $R^*_\alpha = 0.902$ so that the local coordination number is $N_\alpha = 12$. Solutes that occupy β and γ sites are chosen to have $R^*_\beta = 0.799$ and $R^*_\gamma = 0.710$ as required for efficient atomic packing in the first shell of solute-centred clusters with $N_\beta = 10$ and $N_\gamma = 9$, respectively[9]. This model system is designated as <12-10-9> representing the putative coordination numbers of α, β and γ solutes, respectively (Fig. 1b). Clusters with $N = 11$ are not efficiently packed[12,21] and so do not appear in this model. The predicted concentrations (see Methods) and relative sizes of elemental constituents for a <12-10-9> structure provide very good agreement with established bulk metallic glasses based on Zr that contain Be (Fig. 2a). These glass alloys represent several years of study and thousands of alloy iterations, and so are reasonable representations of alloys that provide optimum structural stability in this system, as measured by the maximum thickness of fully amorphous product that can be produced at a fixed cooling rate.

Glass systems are represented by any combination of 1, 2 or 3 solutes with $0.6 \le R \le 1.4$ (the range of R phenomenologically observed in metallic glasses, so that the coordination number N ranges from $8 \le N \le 19$). The convention chosen here is that the largest solutes are α atoms, and β and γ solutes are progressively smaller. Calculating concentrations for a <10-9-8> model thus allows comparison with Ca bulk metallic glasses (Fig. 2b). Again, the present model provides a good prediction of atomic concentrations. Fe-based glasses are commercially the most important and compositionally the most complex, and bulk Fe-based compositions have recently been reported[22,23]. Predictions for a number of Fe-based glasses show very good agreement with actual compositions (Fig. 3). Concentrations have been predicted for other models including <17-12> representing Al-(Ce,Y,La)-(Fe,Co,Cu,Ni) glasses, <16-12> representing Al-Hf-(Fe,Co,Cu,Ni) glasses, <15-12> representing Al-Zr-(Fe,Co,Cu,Ni) glasses, <15-8> representing (Fe,Cr,Mn)-(Mo,W)-(C,B) glasses, <12-10> representing Zr-(Ti,Al,Nb)-(Cu,Ni) glasses, <12-9> representing Pd-(Cu,Ni)-(Si,P) glasses, <10-9> representing (Y,Sm,Nd,La)-Al-(Fe,Co,Cu,Ni) glasses and <10-8> representing Ca-Mg-Cu glasses (see Supplementary Information). With the singular exception of the <12-9> model, the agreement between predicted and observed compositions is similar to that in Fig. 2 and Fig. 3. The capability provided by this structural model to predict the compositions of a wide range of simple and complex metallic glasses is a remarkable achievement. As a result, the present model provides specific guidance for the exploration and discovery of new bulk metallic glasses and replaces the general empirical guidelines established experientially over the past 40 years.

Defects may exist within the dense cluster-packing model. Calculated compositions for <8>, <10> and <17> binary glasses with vacant β and γ sites show very good agreement with experiment (Fig. 2c). Compositions predicted for Mg-Zn and Co-Ti binary glasses with anti-site defects on β sites and vacant γ sites are also shown in Fig. 2c. Anti-site defects can produce a significant range in solute concentrations for some glasses. For example, Mg glasses show a
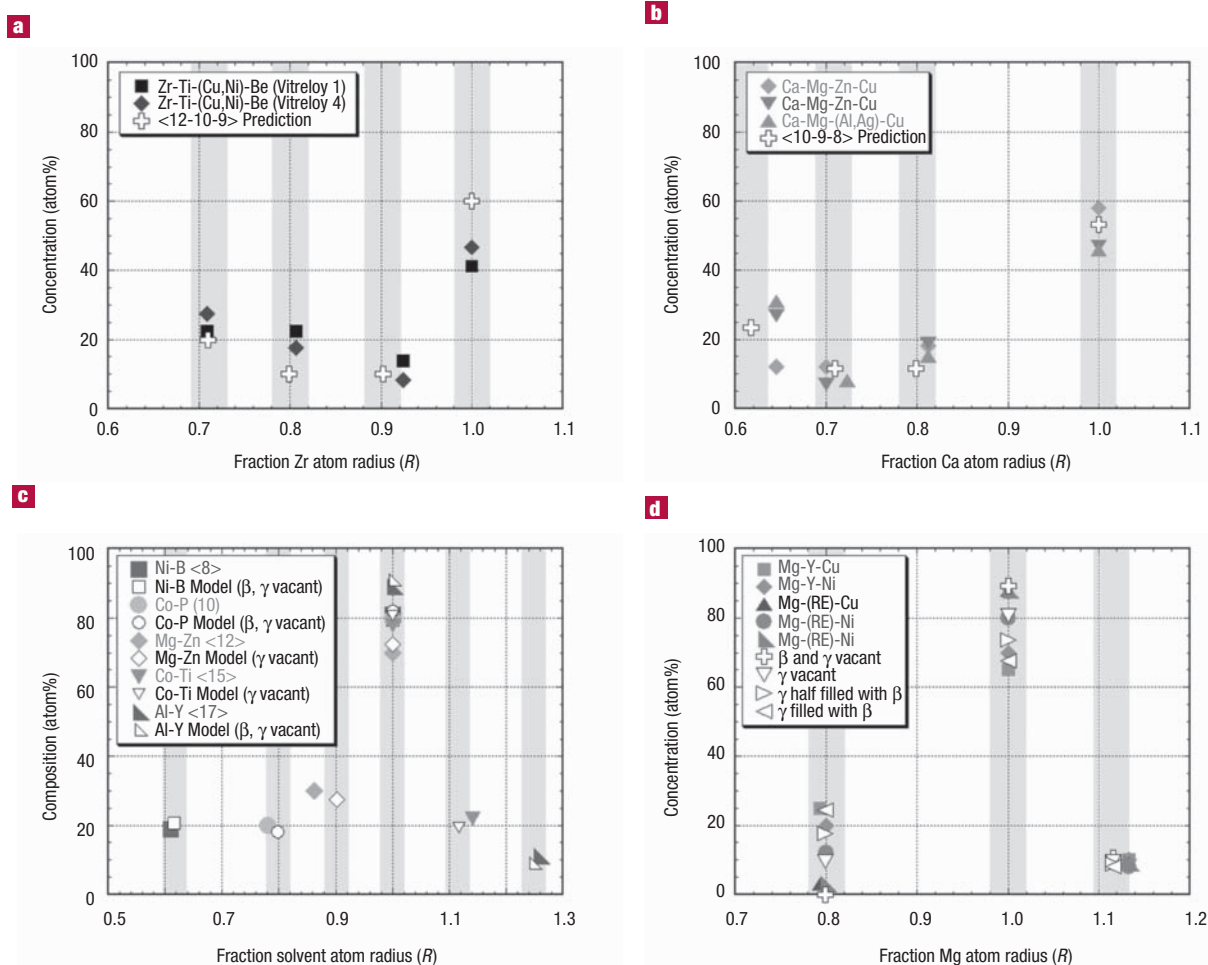
Figure 2 Comparison of relative atomic sizes and concentrations for selected metallic glasses with predictions from the dense cluster-packing model (see ref. 39 for further details of this mode of presentation). Elements enclosed in parentheses in the legends have nearly identical atomic radii and thus represent topologically identical solutes. The concentrations of these atoms are summed in the respective plots. **a**, Zr-based bulk metallic glasses (the commercial Vitlroy 1 and 4) representing <12-10-9>. **b**, Ca-based bulk metallic glasses representing <10-9-8> glasses. **c**, Several binary metallic glasses covering a range of solute sizes. **d**, Mg-based metallic glasses representing <15-10> glasses with rare earth metal (RE) solutes.

significant concentration range for transition metal solute (Fig. 2d). Concentrations are calculated assuming that the α and β sites are filled by the respective solutes, and that vacant γ sites are progressively filled with β solutes. Concentrations are also calculated for topological binary Mg-(Ce,Y) glasses where all β and γ sites are vacant. The concentrations and the concentration range thus predicted show very good agreement with the observed compositions. The best glass-forming alloys are reported to contain 25% of the transition metal[24], consistent with the general observation that the best stability is obtained in structures with filled α, β and γ sites.

Partial (also called differential or environmental) radial distribution functions obtained by diffraction represent experimental data with the highest information content for actual glass structures, and so a credible structural model must show consistency with these data. Predicted solute–solute partial radial distribution functions for an f.c.c. cluster arrangement (see Methods) of several binary glasses are compared with experimental data (Fig. 4). The solutes in $Ni_{63}Nb_{37}$, $Nb_{60}Ni_{40}$ and $Ti_{60}Ni_{40}$ (not shown in Fig. 4) are presumed to occupy all of the α, β and γ sites as suggested from the solute concentrations, and solutes occupy all of the α and β and one half of the γ sites in $Zr_{65}Ni_{35}$.

The $Ni_{81}B_{19}$ glass composition suggests that the β and γ sites are vacant. Nearest-neighbour solute–solute peaks in Fig. 4, curves a–c, indicate the presence of anti-site point defects consisting of α atoms on Ω sites, but a B–B nearest-neighbour peak at ~0.170 nm is absent in Fig. 4, curve d, suggesting that these defects do not occur in $Ni_{81}B_{19}$. Predictions shown in Fig. 4 include solute–solute nearest–neighbour peaks in Fig. 4, curves a–c, to account for these defects. Reasonable agreement for atomic separations extending to a radial distance of about 1 nm is obtained for solute–solute peaks in $Ni_{63}Nb_{37}$ (Fig. 4, curve a) and $Ti_{60}Ni_{40}$, including a faithful representation of the splitting of the first major peak beyond the nearest-neighbour peak. Predicted solute–solute separations for $Nb_{60}Ni_{40}$ (Fig 4b) and $Zr_{65}Ni_{35}$ (Fig. 4, curve c) show good agreement with experimental data to a radial distance of about 0.7 nm. The splitting of the first major peak is not properly predicted for $Ni_{81}B_{19}$, but other solute–solute separations are reasonably well predicted to a radial distance of ~1.0 nm (Fig. 4, curve d). Unlike previous structural models, where a B–B separation nearly twice the equilibrium value and an adjustable domain size were required to produce a reasonable match with data[7], the present fit is obtained without these arbitrary adjustments. Further, the present model provides good agreement for a
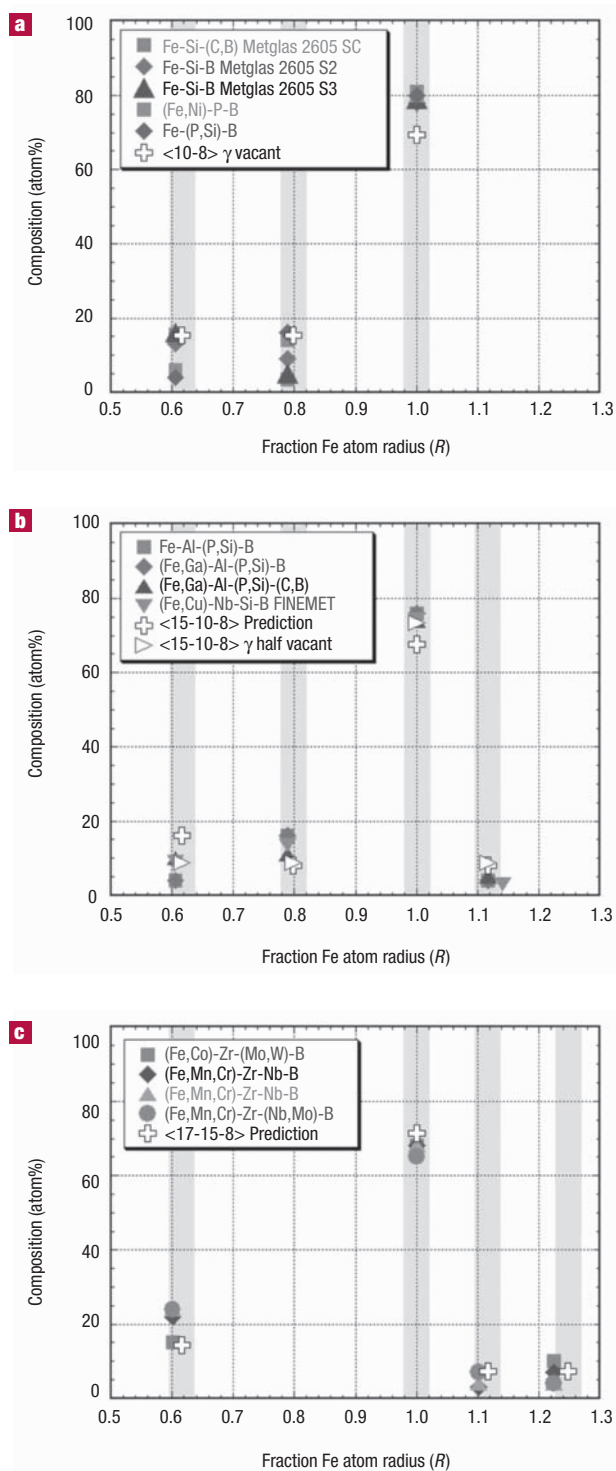
Figure 3 Comparison of relative atomic sizes and concentrations for selected Fe-based metallic glasses with predictions from the dense cluster-packing model (see ref. 39 for further details of this mode of presentation). Elements enclosed in parentheses in the legends have nearly identical atomic radii and thus represent topologically identical solutes. The concentrations of these atoms are summed in the respective plots. **a**, <10-8> glasses including the commercially important Metglas alloys. **b**, <15-10-8> glasses including the commercially important FINEMET alloy. **c**, <17-15-8> glasses, including non-ferromagnetic amorphous steels.

range of topologically distinct glasses (Ni-B is <9>, Zr-Ni is <10>, Nb-Ni and Ti-Ni are <12> and Ni-Nb is <15>), and so represents an important improvement over previous structural models. Thus, an f.c.c. cluster packing provides a meaningful representation of the MRO observed in metallic glasses. Solute symmetry is not supported beyond length scales of ~0.7–1.0 nm due to internal strains (see Methods), but this ordering is nevertheless consistent with the thermodynamic implications of a report for a first-order phase transformation in the nucleation and growth of a metallic glass phase[25].

Inspection of the dense cluster-packing model shows that approximately two each of α, β and γ solutes are first nearest neighbours with a typical Ω atom. Several binary glasses with compositions that suggest a structure with vacant β and γ sites have been considered to explore this prediction, including $Fe_{80}B_{20}$, $Ni_{81}B_{19}$, $Co_{80}P_{20}$ and $Al_{90}Y_{10}$ (refs 26–29, respectively). The measured solvent–solute coordination numbers $N_{\Omega-\alpha}$ for these systems range from 1.6 to 2.2, in good agreement with the expected value of 2. Individual solvent–solute coordination numbers in $Zr_{60}Al_{15}Ni_{25}$, $La_{55}Al_{25}Ni_{20}$, $Zr_{70}Ga_{10}Ni_{20}$ (ref. 30) and $Al_{87}Y_8Ni_5$ (ref. 29). range from 0–3.0, with typical values of 1.3–2.1. $Ni_{64}B_{36}$ suggests a structure where all α and β sites are filled by B (the predicted composition for this structure is $Ni_{66}B_{34}$), so that the solvent–solute coordination number is expected to be ~4. The experimental value of N_{Ni-B} is 4.9 for this glass[31]. $Nb_{60}Ni_{40}$ and $Ni_{63}Nb_{37}$ suggest structures where all α, β and γ sites are occupied by the solute, so that solvent–solute coordination numbers of ~6 are expected. The solvent–solute coordination number is 5.5 for $Nb_{60}Ni_{40}$ and is 5.9 for $Ni_{63}Nb_{37}$ (ref. 32), in good agreement with predictions from the dense cluster-packing model.

Handbook values for atomic radii are generally obtained by providing consistency with measurements in a broad range of metallic, covalent and ionic compounds[33,34]. Although these values generally provide an error of perhaps 5 pm (ref. 34), a somewhat better agreement may be expected for radii optimized for solids dominated by metallic and covalent bonding. Bond lengths in metallic glasses are often shorter than the sum of metallic radii, and so representing atomic size as a ratio of radii also reduces error. Atomic radii used to calculate values of R here are taken from an earlier critical analysis of diffraction measurements in a range of metallic glasses[35] and from a critical assessment of bond lengths given in ref. 36 for selected atom pairs in intermetallic compounds compositionally similar to metallic glasses. Reasonably consistent results are obtained in the present work using these values (and previously given in ref. 9) with a range of ±2% for R. A more complete discussion of probable errors in atomic radii is given in refs 9, 33 and 34.

Elements possessing R values within ±2% of one another are considered topologically equivalent. These solutes are enclosed in parentheses in the alloy designations above and their concentrations are added in these comparisons. Thus, Zr-Al-(Cu,Ni) is a topological ternary alloy because $R_{Ni} \cong R_{Cu}$. Although many glasses were considered here from the literature, with as many as six chemically distinct solutes, alloys with more than three topologically distinct solutes were not identified, further strengthening this feature of the model.

Although discussion of the present structural model has thus far emphasized the influence of atomic size, chemical effects, which appear through the requirement of solvent atoms only in the first coordination shell of efficiently packed solute-centred clusters, provide an important contribution. Indeed, balancing the chemical forces within the structure is expected to play a vital role in the structural stability of glasses[37]. Thus, topologically equivalent but chemically distinct solutes can have different effects on the stability of an amorphous structure. The chemical basis by which a particular solute may improve the stability of an amorphous alloy is still not established, although manifestations such as large negative enthalpies of mixing for stabilizing solutes are well known. The present model is therefore not fully predictive, as a quantitative description of the chemical interaction is
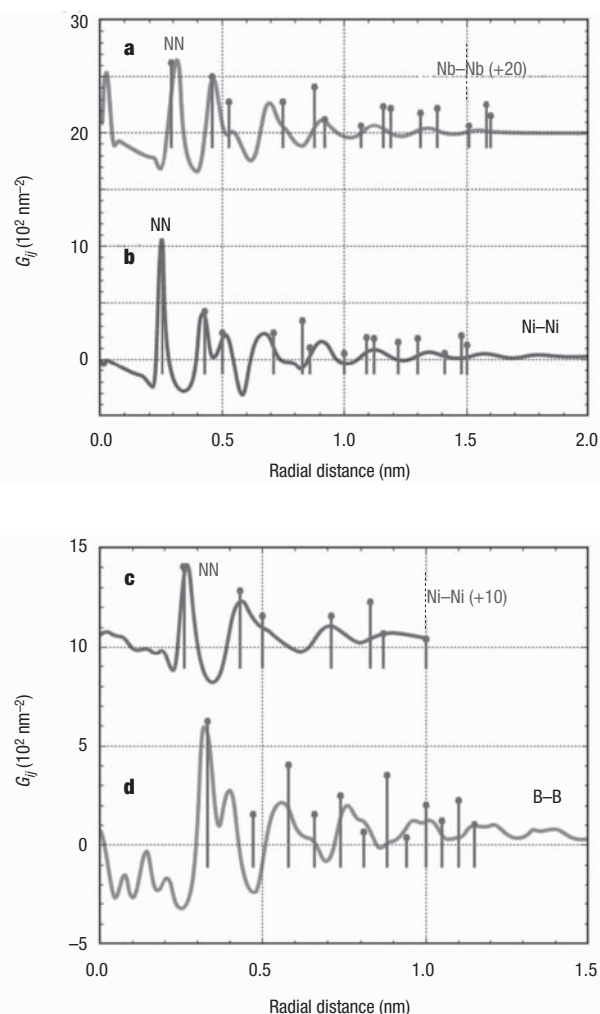
Figure 4 Comparison of predicted and experimental solute–solute reduced partial radial distribution functions (G_{ij}) for selected binary metallic glasses. Specific comparisons are made for **a**, Nb–Nb separations in $Ni_{63}Nb_{37}$. **b**, Ni–Ni separations in $Nb_{60}Ni_{40}$. **c**, Ni–Ni separations in $Zr_{65}Ni_{35}$. **d**, B–B separations in $Ni_{81}B_{19}$. A good fit is seen in all cases up to a radial distance of 0.7–1.0 nm. The solute–solute nearest-neighbour (NN) peaks in **a–c** indicate the presence of anti-site point defects consisting of α solutes occupying Ω sites within the structure. The absence of a B–B nearest-neighbour peak at ~0.170 nm suggests that these defects do not occur in $Ni_{81}B_{19}$. The experimental curves have been redrawn from refs 17, 27 and 40.

necessary to define how topologically equivalent but chemically distinct solutes may enhance or inhibit glass stability.

Although computational techniques provide a powerful approach for seeking insight into the structure and stability of metallic glasses, difficulties are anticipated in comparing earlier results with the present model. The restricted timescales accessible by computation impose quench rates that are higher than experimentally achievable values by 6 to 12 orders of magnitude. As the structure of amorphous systems depends on quench rate, this introduces an important potential error. Reverse Monte Carlo simulations produce structures that show consistency with measured radial distribution functions. Although this consistency is a necessary condition for structural validation, it is not by itself sufficient because consistency can be achieved by a number of

non-equivalent structures. The present model may provide guidance in selection of initial structures, and such studies are now underway.

The dense cluster-packing model briefly described here includes both size and chemical effects, and is summarized by these features: (i) efficiently packed solute-centred atomic clusters with solvent atoms only in the first coordination shell are densely packed to form a structure of overlapping clusters; (ii) three topologically distinct solutes exist: primary cluster-forming solutes (α), cluster-octahedral solutes (β) and cluster-tetrahedral solutes (γ); (iii) all solutes posses radius ratios relative to the solvent, R^*, that enable efficient atomic packing in the first coordination shell; (iv) face-sharing of adjacent clusters is preferred to minimize volume, but edge- and vertex-sharing may exist to reduce internal strains; (v) solutes with atomic radii within ±2% of one another are considered topologically equivalent; and (vi) no orientational order exists between clusters. The dense cluster-packing model is consistent with the full range of phenomenological guidelines established for metallic glasses. An f.c.c. cluster packing provides a reasonable predictive capability for observed medium range order up to a length scale of ~0.7–1.0 nm, and internal strains degrade order beyond this distance. The ability to predict accurately the number of solute atoms in the first coordination shell of a typical solvent atom and to reproduce atomic concentrations in a wide range of metallic glasses provides a convincing validation and is a remarkable achievement of this model. In the near term, this model provides specific guidance for the exploration and development of bulk metallic glasses by offering a structural basis for the selection of candidate solute elements and concentrations. This model may also provide mechanistic insights into processes such as deformation and mass transport in metallic glasses. In the longer term, this sphere-packing scheme may provide insight into other scientific problems where the efficient filling of space by spheres of unequal size is important.

METHODS

CALCULATION OF CLUSTER LATTICE UNIT CELL LENGTH Λ_0

Atomic packing along <100> of a cluster unit cell is represented as α–Ω–β–Ω–α, along <110> as α–Ω–α–Ω–α and along <111> as α–Ω–γ–Ω–β–Ω–γ–Ω–α. The densest packing occurs when adjacent clusters share faces. Because equilateral triangular arrangements of solvent atoms provide the most efficient packing in the first coordination shell, nearest-neighbour solutes for adjacent face-sharing clusters occupy opposite caps of a trigonal bipyramid. Solute separation can thus be obtained from geometry, and the lengths along <100>, <110> and <111> directions are given by

$$d_{<100>} = 2r_\Omega \left[\sqrt{(R_\alpha+1)^2 - 4/3} + \sqrt{(R_\beta+1)^2 - 4/3} \right]$$

$$d_{<110>} = 4r_\Omega \left[\sqrt{(R_\alpha+1)^2 - 4/3} \right]$$

$$d_{<111>} = 2r_\Omega \left[\sqrt{(R_\alpha+1)^2 - 4/3} + \sqrt{(R_\beta+1)^2 - 4/3} + 2\sqrt{(R_\gamma+1)^2 - 4/3} \right]$$

The cluster unit cell length for f.c.c. packing of primary clusters Λ_0 is obtained from the lengths $d_{<100>}$, $d_{<110>}/\sqrt{2}$ and $d_{<111>}/\sqrt{3}$. Three different values of Λ_0 are generally obtained, and the largest value is used for comparison with experiment.

CONSTITUENT CONCENTRATION CALCULATIONS

Consider any system where $N_\alpha = 12$ and all β and γ sites are occupied by β and γ solutes, such as <12-10-9> or <12-9-8>. An f.c.c. arrangement of α clusters provides 1 β site and 2 γ sites for each α site. The 12 Ω atoms in a given α cluster are shared between the central α solute and the 12 nearest-neighbour α clusters in the f.c.c. lattice, so that there are a net 6 Ω atoms per α solute. There are thus a total of 10 atoms per α site and the atomic concentrations are $C_\alpha = 10\%$, $C_\beta = 10\%$, $C_\gamma = 20\%$ and $C_\Omega = 60\%$. Appropriate changes are made for anti-site defects, so that a <12-10> system where all γ sites are occupied by β solutes will have concentrations $C_\alpha = 10\%$, $C_\beta = 30\%$ and $C_\Omega = 60\%$. Finally, a system with vacant sites will have a smaller total number of atoms per α site, so that a binary <12> glass where all β and γ sites are vacant will have a total of 7 atoms per α site with concentrations $C_\alpha = 14.3\%$ and $C_\Omega = 85.7\%$. For glass systems where $N_\alpha \neq 12$ the number of Ω atoms per α solute is generalized as $[N_\alpha/(1+(12/N_\alpha)]$, where 12 represents the number of nearest-neighbour α clusters in an f.c.c. lattice.

CALCULATION OF SOLUTE–SOLUTE SEPARATIONS FOR RADIAL DISTRIBUTION FUNCTIONS

The multiplicity and distribution in radial distances from a particular solute site to all other similar sites in a cluster unit cell is obtained from geometry[38] and from Λ_0. For example, nearest-neighbour α solutes occur along 1/2<110> so that the minimum α–α separation is $d_{<110>}/2 = \Lambda_0/\sqrt{2}$, and nearest-neighbour γ solutes occur along 1/2<100> so that the minimum γ–γ separation is $d_{<100>}/2 = \Lambda_0/2$. Both α and β sites

occupy points of an f.c.c. lattice of unit length Λ_0, so that α–α and β–β radial distribution functions are identical. On the other hand, γ sites occupy points of a simple cubic lattice of unit length $\Lambda_0/2$ so that radial distribution functions for γ–γ separations provide a different result. A simple cubic lattice of unit length $\Lambda_0/2$ is also produced when a single solute species occupies both α and β sites, so that solute–solute separations in this case are identical to the γ–γ radial distribution function. Finally, when all three solute sites are occupied by a single solute species, solute–solute separations are calculated from a body-centred-cubic cell of unit length $\Lambda_0/2$.

References

1. Klement, W., Willens, R. H. & Duwez, P. Non-crystalline structure in solidified gold-silicon alloys. *Nature* **187,** 869–870 (1960).
2. Bernal, J. D. & Mason, J. Co-ordination of randomly packed spheres. *Nature* **188,** 910–911 (1960).
3. Scott, G. D. Packing of spheres. *Nature* **188,** 908–909 (1960).
4. Finney, J. L. Random packings and the structure of simple liquids I. The geometry of random close packing. *Proc. Roy. Soc. Lond. A* **319,** 479–493 (1970).
5. Gaskell, P. H. A new structural model for transition metal-metalloid glasses. *Nature* **276,** 484–485 (1978).
6. Gaskell, P. H. A new structural model for amorphous transition metal silicides, borides, phosphides and carbides. *J. Non-Cryst. Solids* **32,** 207 (1979).
7. Dubois, J. M., Gaskell, P. H. & Le Caer, G. A model for the structure of metallic glasses based on chemical twinning. *Proc. Roy. Soc. A* **402,** 323–357 (1985).
8. Gaskell, P. H. in *Materials Science and Technology* (ed. Zarzycki, J.) 175–278 (VCH, Cambridge, UK, 1991).
9. Miracle, D. B., Sanders, W. S. & Senkov, O. N. The influence of efficient atomic packing on the constitution of metallic glasses. *Phil. Mag. A* **83,** 2409–2428 (2003).
10. Miracle, D. B. & Senkov, O. N. A geometric model for atomic configurations in amorphous Al alloys. *J. Non-Cryst. Solids* **319,** 174–191 (2003).
11. Miracle, D. B. Efficient local packing in metallic glasses. *J. Non-Cryst. Solids* (in the press).
12. Mackay, A. L., Finney, J. L. & Gotoh, K. The closest packing of equal spheres on a spherical surface. *Acta Crystallogr.* **A33,** 98–100 (1977).
13. Clare, B. W. & Kepert, D. L. The optimal packing of circles on a sphere. *J. Math. Chem.* **6,** 325–349 (1991).
14. Sloane, N. J. A. Kepler's conjecture confirmed. *Nature* **395,** 435–436 (1998).
15. Gaskell, P. H. in *Glassy Metals II* (eds Beck, H. & Guntherodt, H.-J.) 5–49 (Springer, Berlin, Germany, 1983).
16. Sietsma, J. & Thijsse, B. J. An investigation of universal medium range order in metallic glasses. *J. Non-Cryst. Solids* **135,** 146–154 (1991).
17. Lamparter, P. & Steeb, S. in *Structure of Solids* (ed. Gerold, V.) 217–288 (VCH, Weinheim, Germany, 1993).
18. Hufnagel, T. C. & Brennan, S. Short- and medium-range order in $(Zr_{70}Cu_{20}Ni1_0)_{90-x}Ta_xAl_{10}$ bulk amorphous alloys. *Phys. Rev. B* **67,** 014203 (2003).
19. Gaskell, P. H. On the structure of simple inorganic amorphous solids. *J. Phys. C Phys.* **12,** 4337–4368 (1979).
20. Stephens, P. W. in *Extended Icosahedral Structures* (eds Jaric, M. V. & Gratias, D.) 37–104 (Academic, Boston, Massachusetts, USA, 1989).
21. Aste, T. & Weaire, D. *The Pursuit of Perfect Packing* (Institute of Physics, Bristol, UK, 2000).
22. Ponnambalam, V. *et al.* Synthesis of iron-based bulk metallic glasses as nonferromagnetic amorphou steel alloys. *Appl. Phys. Lett.* **83,** 1131–1133 (2003).
23. Ponnambalam, V., Poon, S. J. & Shiflet, G. J. Fe-based bulk metallic glasses with diameter thickness larger than one centimeter. *J. Mat. Res.* **19,** 1320–1323 (2004).
24. Inoue, A., Kato, A., Zhang, T., Kim, S. G. & Masumoto, T. Mg-Cu-Y amorphous alloys with high mechanical strengths produced by a metallic mold casting method. *Mater. Trans. JIM* **32,** 609–616 (1991).
25. Cahn, J. W. & Bendersky, L. A. in *Amorphous and Nanocrystalline Metals* (eds Busch, R. *et al.*) 139–143 (Materials Research Society, Warrendale, Pennsylvania, 2004).
26. Nold, E., Lamparter, P., Olbrich, H., Rainer-Harbach, G. & Steeb, S. Determination of the Partial Structure Factors on the Metallic Glass $Fe_{80}B_{20}$. *Z. Naturforsch.* **36a,** 1032–1044 (1981).
27. Lamparter, P., Sperl, W., Steeb, S. & Bletry, J. Atomic structure of amorphous metallic $Ni_{81}B_{19}$. *Z. Naturforsch.* **37a,** 1223–1234 (1982).
28. Sadoc, J. F. & Dixmier, J. Structural investigation of amorphous CoP and NiP Alloys by combined X-ray and neutron scattering. *Mater. Sci. Eng.* **23,** 187–192 (1976).
29. Matsubara, E., Waseda, Y., Inoue, A., Ohtera, H. & Masumoto, T. Anomalous X-ray scattering on amorphous $Al_{87}Y_8Ni_5$ and $Al_{90}Y_{10}$ alloys. *Z. Naturforsch.* **44a,** 814–820 (1989).
30. Matsubara, E. & Waseda, Y. Structural studies of new metallic amorphous alloys with wide supercooled liquid region (Overview). *Mater. Trans. JIM* **36,** 883–889 (1995).
31. Cowlam, N., Guoan, W., Gargner, P. P. & Davies, H. A. $Ni_{64}B_{36}$ - A transition metal-metalloid glass with first neighbor metalloid atoms. *J. Non-Cryst. Solids* **61-62,** 337–342 (1984).
32. Steeb, S. & Lamparter, P. Structure of binary metallic glasses. *J. Non-Cryst. Solids* **156–158,** 24–33 (1993).
33. Pauling, L. *The Nature of the Chemical Bond* (Cornell Univ. Press, Ithaca, NewYork, 1960).
34. Slater, J. C. Atomic radii in crystals. *J. Chem. Phys.* **41,** 3199–3204 (1964).
35. Egami, T. & Waseda, Y. Atomic size effect on the formability of metallic glasses. *J. Non-Cryst. Solids* **64,** 113–134 (1984).
36. Daams, J. L. C., Villars, P.& van Vucht, J. H. N. *Atlas of Crystal Structure Types for Intermetallic Phases* (ASM, International, Metals Park, Ohio, 1991).
37. Poon, S. J., Shiflet, G. J., Guo, F. Q. & Ponnambalam, V. Glass formability of ferrous- and aluminum-based structural metallic alloys. *J. Non-Cryst. Solids* **317,** 1–9 (2003).
38. Kasper, J. S. & Lonsdale, K. (eds) *International Tables for X-Ray Crystallography* (Kluwer Academic, Dordrecht, Holland, 1989).
39. Senkov, O. N. & Miracle, D. B. Effect of the atomic size distribution on glass forming ability of amorphous metallic alloys. *Mater. Res. Bull.* **36,** 2183–2198 (2001).
40. Lee, A., Etherington, G. & Wagner, C. N. J. Partial structure functions of amorphous $Ni_{35}Zr_{65}$. *J. Non-Cryst. Solids* **61-62,** 349–354 (1984).

Competing financial interests

The author declares that he has no competing financial interests.